Pramana – J. Phys., Vol. 37, No. 6, December 1991, pp. 457–488. © Printed in India.

Geometrical theory of diffraction

P B SUNIL KUMAR and G S RANGANATH
Raman Research Institute, Bangalore 560080, India

MS received 25 September 1991; revised 14 October 1991

Abstract. Geometrical theory of diffraction (GTD) is an alternative model of diffraction propounded first by Thomas Young in 1802. GTD has a long history of nearly 150 years over which many eminent people enriched this model which has now become an accepted tool in the calculation of diffraction patterns. In the conventional Helmholtz–Kirchhoff theory the diffracted field is obtained by computing the net effect of the waves emitted by all points within the area of the aperture. But GTD reduces this problem to one of computing the net effect of waves from a few points on the boundary of the aperture or obstacle, thus simplifying considerably the labour involved in computations. Also the theory can easily be modified to include polarization effects. This has been done specifically by Keller (1962) who exploited the Sommerfeld solution of diffraction of electromagnetic waves at a half plane, making the theory more versatile than the Kirchhoff scalar wave theory. Interestingly the geometry of diffracted rays is predictable from a generalized Fermat principle. According to this the total path chosen by light from the source to the point of observation via the diffracting boundary is an extremum. Historically it should be stated that many of the salient features of GTD were established by a school led by Raman which was active from 1919–1945. Later when Keller (1962) revived GTD independently, he and others who followed him rediscovered many of the results of the Raman school. We have stressed wherever necessary the contributions of the Indian School. We have also discussed certain geometries where GTD can be effectively used. We get some new and interesting results, which can be easily understood on GTD, but are difficult to interpret on the conventional theory of diffraction.

Keywords. Diffraction; Fresnel diffraction; boundary waves.

PACS Nos 42·10; 42·20; 42·30

Table of contents

1. Introduction

Maxwell's electromagnetic theory is undoubtedly the most important contribution to our understanding of light. At one stroke it could easily explain the phenomena of interference, diffraction and polarization of light. In particular, the study of polarization and diffraction got a new impetus. Since light obeys Maxwell's equations, many great physicists from Lord Rayleigh to Sommerfeld tried to get everything about light from these equations. In these attempts both the power as well as the limitations of this approach became quickly obvious. For all their mathematical beauty, the partial differential equations of Maxwell were not easy to solve in every given problem. The practical difficulties forced many to think of other ways of solving some of the formidable problems particularly in the domain of optical diffraction.

The fact that *light* in many ways behaved like *sound* was exploited by a few to break new ground in this field. For example, the first mathematical theory of light diffraction is due to Fresnel. He reaffirmed the wave nature of light and gave a theory of half-period zones with which he could calculate diffraction patterns in simple geometries. This gave remarkable agreement with experiments.

Kirchhoff's theory of diffraction of sound waves was extended to the domain of *light*. This exercise was not without its failures. It leads to many computational difficulties when applied to even slightly complicated geometries. Using Kirchhoff's integral we can in principle calculate the diffraction patterns of apertures and obstacles. The procedure is tedious and time-consuming. In figure 1 we show the diffraction patterns obtained on a computer with this technique, for equilateral triangular apertures at fixed distance from the screen. It clearly brings out the experimentally observed features. Also we do recognize the gradual transition from a Fresnel pattern of three-fold symmetry to a Fraunhofer pattern of six-fold symmetry. But purists were constantly besieged by the fact that it was a scalar wave theory and was thus strictly speaking incapable of handling electromagnetic waves.

It is these technical difficulties that make *diffraction problems* hard to solve. And wherever one got answers, a physical understanding was still elusive. This became apparent even in one of the earliest problems, viz., diffraction at a circular disk. Though Poisson predicted from Fresnel's theory a bright spot at the centre of the shadow of a circular disk, he refused to believe it and used the result as an argument to reject Fresnel's theory of diffraction. Fortunately, Arago's experimental demonstration of this phenomenon saved Fresnel's theory.

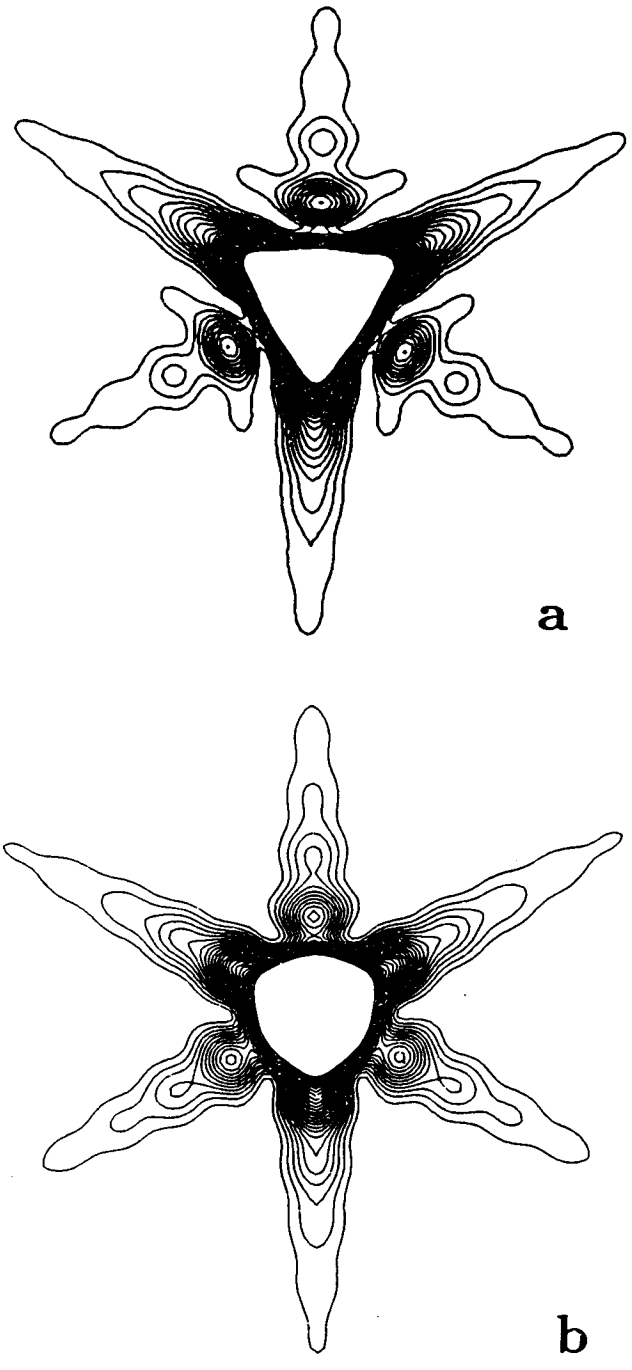

Figure 1.

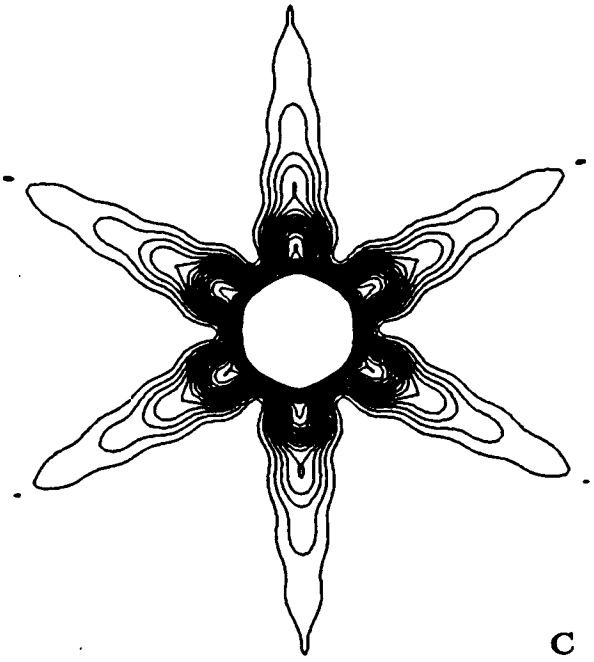

Figure 1. Diffraction intensity contour maps of an equilateral triangular aperture calculated using Kirchoff theory at a distance of 100 cm. Triangular apertures are of side (a) 1 cm, (b) 0·06 cm, (c) 0·01 cm.

Only against such a background we can appreciate the alternative model of diffraction, which was first propounded by Thomas Young (1802). Young's theory evolved out an interesting experimental observation. Even from deep within the shadow, a straight edge appears as a luminous line, and diffraction fringes associated with edges are seen only outside the shadow region. Young argued that these two facts can be explained by assuming that the edge emits waves in all directions. Outside the shadow boundary it interferes with the main geometrically transmitted wave, resulting in a fringe pattern and inside the shadow one gets a monotonic decrease in intensity. Though Young laid the foundations of a new theory of diffraction, it took many decades to work out the details that were necessary for its application to objects of arbitrary shape. It also became very important to make contacts with the Kirchhoff theory in view of its successes in the early years of diffraction theory. In addition, the inclusion of the polarization of the electromagnetic waves was neither easy nor straightforward. One had to appeal to typical solutions of Maxwell's equations to incorporate polarization effects. All this ultimately lead to the establishment of the geometrical theory of diffraction (GTD). In essence it is a recapitulation of Young's idea, viz., diffraction is a manifestation of interference between the directly transmitted light waves and waves emitted by the boundary of the diffracting object.

From the point of view of mathematical computations this theory is quite simple and straightforward. Also it is possible to easily and physically account for many strange and peculiar facts associated with diffraction patterns. For example, the Poisson spot associated with a circular disk is due to a constructive interference at the centre of the waves emanating from the circular boundary. In spite of all these

attractive features, GTD is still an approximate theory and it does not go over to the Fraunhofer diffraction limit. Its power lies in its utility as a tool to get quickly and to a reasonable accuracy the Fresnel diffraction patterns of objects and apertures of arbitrary shapes. It should be emphasized that calculations based on the Kirchhoff theory are very cumbersome since they involve oscillatory integrals. This results in substantial cancellations to the net effect. In GTD these cancellations isolate the points that make the important contributions to the diffraction pattern.

GTD has played a very important role in the computation of fields diffracted from macroscopic objects due to incident radio waves. In many radio engineering problems like antenna design we need to know the strength and structure of the scattered field. Since a solution based on electrodynamic equations is not easily obtainable, GTD techniques come in handy. This has recently been dealt with exhaustively by McNamara *et al* (1990). In this article, however, we shall not dwell upon these engineering problems but will confine ourselves to situations that arise in the region of wavelengths small compared with the size of the diffracting screen. Also we present some interesting results that have emerged out of the application of GTD to certain optical problems.

It is also of historical importance to notice that many of the essential steps of GTD were rediscovered by many succeeding investigators. In this context particular mention should be made of the contributions of the school lead by Raman. Over a period of nearly thirty years they worked out the important aspects of GTD. But all these investigations appear to have gone unnoticed by the later workers who revived Young's theory of diffraction. We have emphasized elsewhere the work of the Indian School in this field (Sunil Kumar and Ranganath 1991).

2. Boundary wave theory of diffraction

Young's model of diffraction proposed in 1802 lay dormant for nearly the next hundred years. This may partly be due to Fresnel's criticism that Young's theory was not amenable to quantitative analysis. But in 1888 Maggi showed that the Kirchhoff diffraction integral (which is a superior mathematical formulation of diffraction to Fresnel's theory of half period zones) may be reduced to a sum of (i) a wave propagating according to the laws of geometrical optics called the geometrical wave, and (ii) a wave originating from every point on the boundary of the obstacle or aperture – called the boundary wave. This is reminiscent of Young's theory. In 1896, Sommerfeld, without being aware of Maggi's work, solved the problem of electromagnetic diffraction at a perfectly conducting half plane in the framework of Kirchhoff theory. Interestingly he got a solution similar to the one obtained by Maggi. The field at any point can be looked upon as the sum of a geometrically transmitted wave and a cylindrical wave diverging from the straight edge. Sommerfeld gave a new life to Young's theory and many followed him in elaborating on this *boundary wave* theory of diffraction. In view of their significance we shall briefly present here the various important problems solved by different workers.

2.1 *Diffraction by a straight wedge*

Let Z axis be along the edge of a wedge. The wedge is described by a sector of interior angle $(2\pi - \beta)$ (see figure 2). The incident ray is along $\phi = \phi_0$. The geometrically

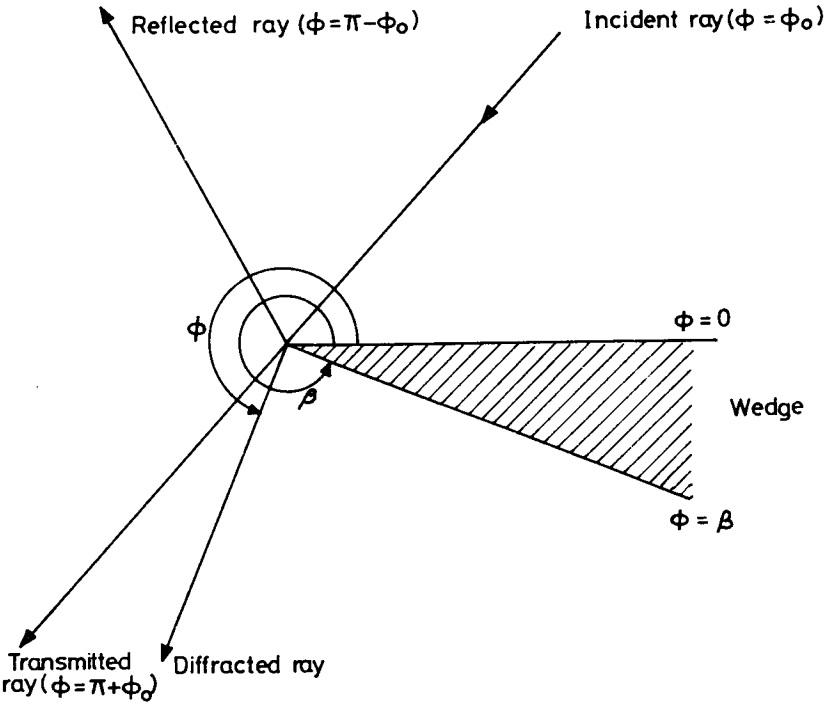

Figure 2. Diffraction geometry for rays incident on a straight wedge at a glanching angle of $\phi = \phi_0$. Angle of the wedge is $(2\pi - \beta)$.

reflected and the directly transmitted rays are respectively along $\phi_r = \pi - \phi_0$ and $\phi_t = \pi + \phi_0$.

Then the electromagnetic field in all space is given by

$$u(r, \phi) = v(r, \phi - \phi_0) \mp v(r, \phi + \phi_0)$$

with negative sign for the electric vector parallel to the edge and the positive sign for the electric vector perpendicular to the edge. The function v can be shown to be

$$v(r, \theta) = v_g(r, \theta) + v_d(r, \theta).$$

Here v_g represents the incident or the reflected wave as given by geometrical optics and v_d represents the diffracted wave originating from the edge of the wedge. At distances r (from the edge) large compared to the wavelength it is given by

$$v_d(r, \theta) = \frac{\pi}{\beta(2\pi kr)^{1/2}} \exp[i(kr + \pi/4)] \frac{\sin(\pi^2/\beta)}{\cos(\pi^2/\beta) - \cos(\pi\theta/\beta)}$$

provided

$$\left[\cos\left(\frac{\pi^2}{\beta}\right) - \cos\left(\frac{\pi\theta}{\beta}\right)\right]^2 \gg \frac{1}{kr}.$$

Hence for a half plane ($\beta = 2\pi$)

$$v_d = -\frac{1}{2(2\pi kr)^{1/2}} \exp[i(kr + \pi/4)] \frac{1}{\cos(\theta/2)} \quad \text{for } \cos\theta/2 \gg \frac{1}{(kr)^{1/2}}$$

when $kr \ll 1$

$$v_d = 2(2/\pi)^{1/2} \exp(-i\pi/4)(kr)^{1/2} \sin(\phi_0/2) \sin\theta/2$$

showing that the field is continuous at $r = 0$.

We can also calculate using Maxwell's equations the magnetic field of the diffracted wave. For $kr \gg 1$ we find $H_\alpha = -E_z$ and $H_r = 0$ while for $kr \ll 1$, H_x and H_y diverge like $1/\sqrt{r}$ excepting at $\phi = \pi$ at which $H_x = -\sin\phi_0 \exp(ikr\cos\phi_0)$ and at $\phi = 0, 2\pi$ when $H_y = 0$.

Also it can be shown that for the electric vector parallel to the edge the diffraction field vanishes on the two surfaces of the conducting wedge, i.e., at $\phi = 0$ and $\phi = \beta$.

We can also get directly from Kirchhoff's integral the structure of the edge radiation diffracted at angle of θ for a straight edge. This turns out to be

$$v_d = \frac{\sqrt{2}}{(\pi k)^{1/2}} \exp(-i\pi/4) \frac{\cos\theta}{\tan\theta} \frac{\exp(ikr)}{\sqrt{r}},$$

which is not the same as the Sommerfeld solution.

The Sommerfeld solution, however, is not valid in the close neighbourhood of the incident shadow boundary and reflection shadow boundary, i.e., $\phi = \pi \pm \phi_0$ in view of the divergence in the diffraction field v_d. These difficulties of edge diffraction were overcome in the uniform theory of diffraction which was developed in 1974 by Kouyoumjian and Pathak. They found by an asymptotic analysis that by multiplying v_d by a transition function the diffraction fields can be bounded across the boundaries $\phi = \pi \pm \phi_0$. For a half plane we get

$$v_d(r, \phi) = -\frac{\exp(-i\pi/4)}{2(2\pi k)^{1/2}} \left\{ \frac{F[kra(\phi - \phi_0)]}{\cos(\phi - \phi_0)/2} \mp \frac{F[kra(\phi + \phi_0)]}{\cos(\phi + \phi_0)/2} \right\} \left\{ \frac{\exp(ikr)}{\sqrt{r}} \right\}.$$

Here

$$a(\phi \pm \phi_0) = 2\cos^2(\phi + \phi_0)/2$$

$$F(x) = \text{Transition function} = 2i\sqrt{x} \exp(ix) \int_{\sqrt{x}}^{\infty} \exp(-i\omega^2) d\omega.$$

When the diffracted ray is not close to $\phi = \pi \pm \phi_0$, $F(x) \to 1$ and we get the Sommerfeld solution.

The fact that v_d has a factor $\exp(ikr)/\sqrt{r}$ indicates that it resembles a cylindrical wave emitted by the edge of the wedge. The trigonometric factor indicates a phase jump of π as we cross the shadow boundaries. This led Banerji (1919) to conclude that there is an edge dislocation in the wavefront pattern of the cylindrical wave. Kalaschnikov (1912) showed that these rays can be photographed. He inserted pins into a photographic plate which he then placed at an angle to the ray directions. A long exposure revealed radially directed shadows of these pins on the plate.

Though the Sommerfeld solution could account for the experimentally observed diffraction pattern at a straight edge, it did not give the right polarization features associated with such a phenomenon. Raman and Krishnan (1927) argued that this is due to its inherent assumption that the diffracting screen is made of a perfect conductor (infinite conductivity). They accordingly modified the Sommerfeld theory by writing $u(r, \phi)$ as

$$u(r, \phi) = v_d(r, \phi - \phi_0) \pm \hat{R} v_d(r, \phi + \phi_0).$$

Here $\hat{R}$ is the complex reflection coefficient of the metal of which the diffracting screen is made. Interestingly this simple correction completely accounted for the experimentally observed polarization features. Later experimental work of Savornin (1939) further established the validity of this modification.

2.2 *Diffraction by a thin edge of arbitrary shape*

A similar electrodynamic boundary wave model of diffraction at boundaries of arbitrary shape is yet to be developed. However, much progress has been made in the case of scalar wave diffraction at such boundaries. This is largely due to the fact that the starting point for such models has been the Kirchhoff's theory which can be used for an aperture or an obstacle of any shape. Maggi (1888) was the first to realize that the Kirchhoff's surface integral over the aperture could be reduced to a line integral over the boundary of the aperture together with a contribution corresponding to the geometrically transmitted wave. In fact this work precedes the Sommerfeld analysis but unfortunately remained unnoticed by majority of later workers. Rubinowicz (1917, 1924) independently came to the same conclusions many years later.

With incident spherical waves the Kirchhoff surface integral becomes:

$$v = \frac{1}{4\pi}\int_0 \left\{\frac{\exp(ikr)}{r}\frac{\partial}{\partial n}\frac{\exp(ik\rho)}{\rho} - \frac{\exp(ik\rho)}{\rho}\frac{\partial}{\partial n}\frac{\exp(ikr)}{r}\right\}d\sigma$$

where $\hat{n}$ is the outward surface normal to σ the surface spanning the aperture, r and ρ are the distances of the point of integration from the point of observation P and the light source P_0 respectively. The surface σ together with the diffracting screen will separate the region containing P from that containing P_0.

One point to be noticed in Kirchhoff's theory is that the surface σ can be entirely arbitrary excepting for the condition that it is limited by the curve 's' which forms the boundary of the aperture. Hence the above integration depends only on 's' and not on σ. We now consider the cone formed by the rays emitted by the source and the boundary of the aperture. Let Σ be this conical surface with surface element $d\Sigma$. Then it is easy to show that for points within the volume defined by σ and Σ

$$v = \frac{\exp(ik\rho)}{\rho} - \frac{1}{4\pi}\int I'\,d\Sigma$$

and for exterior points

$$v = -\frac{1}{4\pi}\int I'\,d\Sigma$$

I' is the integrand in the Kirchhoff's integral.

Further the surface integral on Σ can be simplified to a line integral on 's' the edge of the aperture. This is given by

$$\frac{1}{4\pi}\int_s \left\{\frac{\exp(ik\rho)}{\rho}\frac{\exp(ikr)}{r}\frac{\cos\theta_1}{1+\cos\theta_3}\sin\theta_2\right\}ds.$$

The first factor gives the wave incident on the edge and the second factor corresponds to the spherical wave *reflected* by the edge. Also

θ_1 = Angle of reflection at the cone surface,
θ_2 = Angle of incidence at the curved element of the edge,
θ_3 = Angle of reflection at the edge.

Rubinowicz (1917, 1924) further simplified the contour integral by the method of stationary phases. A substantial contribution to the line integral comes from only those points on the contour at which the phase is stationary with respect to a movement on the curve 's'. The phase factor $[k(r + \rho)]$ remains constant on the contour only when

$$\frac{d\rho}{ds} = -\frac{dr}{ds}$$

i.e.,

$$\cos\theta_2 = -\cos\theta_3.$$

This is often referred to as the *reflection condition.* Each of such points at which phase is stationary contributes considerable intensity to the point of observation. The rays that are diffracted by the edge obeying the above reflection condition have been depicted in figure 3, for normal and oblique incidence of incident rays. The cone of

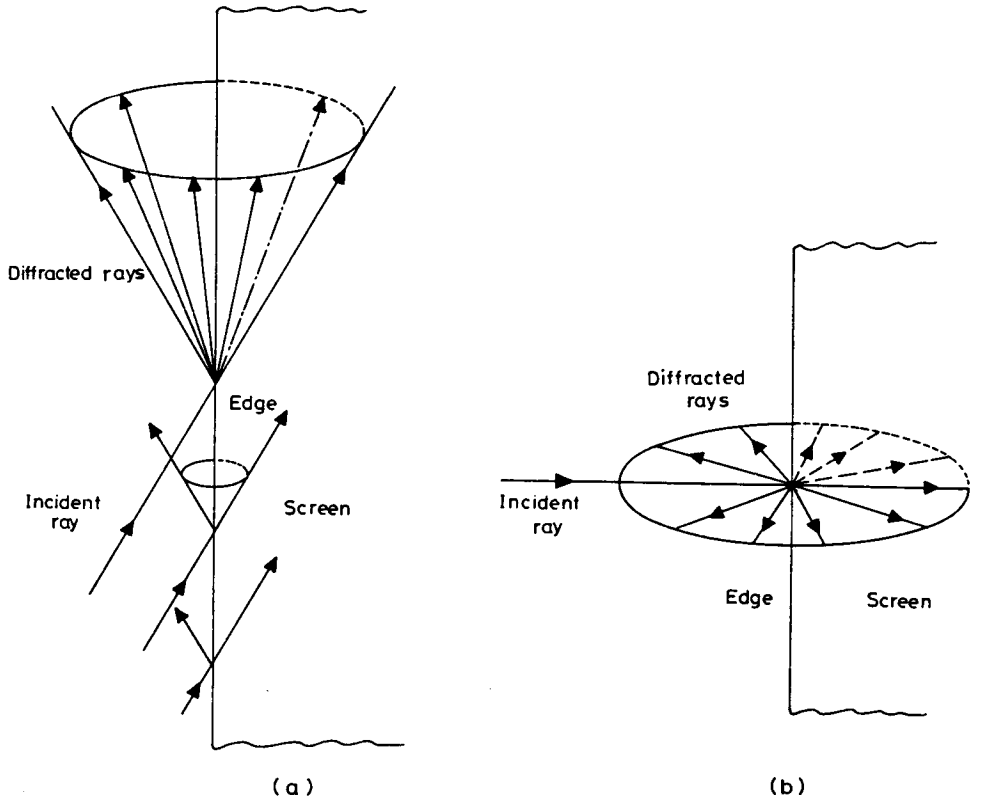

Figure 3. Diffracted rays in Rubinowicz reflection condition. (**a**) Diffracted rays will be on a cone symmetric about the edge for an oblique incidence, (**b**) diffracted rays will be on a disk perpendicular to the edge for normal incidence.

diffracted rays in the case of oblique incidence has been seen experimentally by Maey (1893).

In this context it is important to mention that Raman (1941) obtained essentially the same result by a far simpler procedure. By ignoring the obliquity factor of Kirchhoff's theory, an approximation quite valid in real situations, we get

$$v = \frac{A}{\lambda}\int_{\sigma}\frac{\exp[i(kr)]}{r}\mathrm{d}\sigma.$$

Then it can be shown that

$$v = -\frac{A}{2\pi}\int_{s}\frac{\sin\phi}{r\sin\theta}\exp(ikr)\mathrm{d}s + \frac{\exp(ik\rho)}{\rho}.$$

Here ϕ is the angle that the line element ds at B makes with the plane P_0BP and θ is the angle between the incident ray reaching the line element at B and the diffracted ray reaching the point of observation from this line element as shown in figure 4. The boundary disturbance can be looked upon as being due to light sources of strength $(A\sin\phi)/(2\pi\sin\theta)$ having a phase opposite to that of direct light at the boundary. The maximum contribution to v comes from the line elements for which $\sin\phi$ is a maximum. Therefore the diffracted radiations principally originate at points on the edge where the line element ds is perpendicular to the rays reaching the points of observation.

Hence this analysis indicates that at any point of observation we get spherical waves from a finite number of points on the boundary of an aperture. This fact was experimentally demonstrated by Raman (1919). It is necessary to point out that radiations from these special points which Raman referred to as *poles* are added with appropriate phases at the point of observation. In addition we need also add the geometrically transmitted ray if it also happens to reach the point of observation.

Thus Young's model of diffraction can be theoretically justified within the framework of the Helmholtz–Kirchhoff scalar wave model. It should be mentioned in

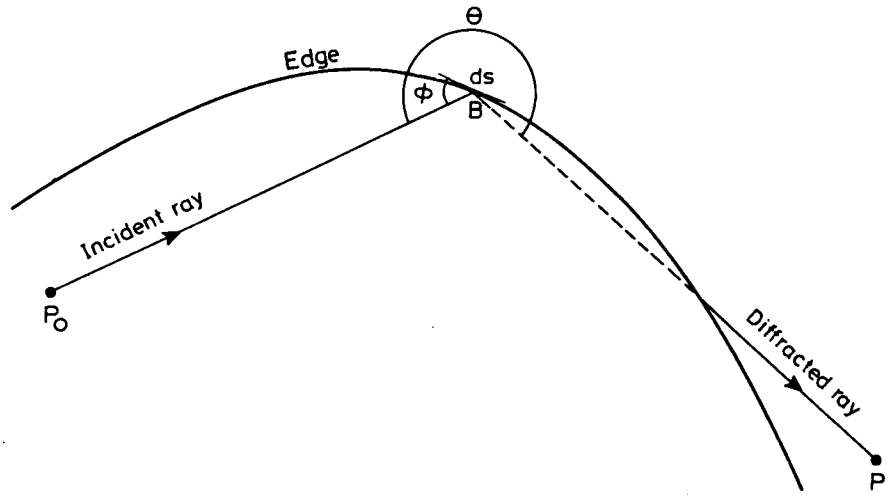

Figure 4. Geometry of diffraction at an aperture.

passing that a similar exercise is also valid for Fraunhofer diffraction. Laue (1936) showed that the Fourier transform integral over the aperture can be reduced to an integral taken round the boundary of the aperture. The Fraunhofer diffraction amplitude is given by

$$v = \int_{-\infty}^{+\infty} f(x, y)\exp[i(k_x x + k_y y)]\mathrm{d}x\mathrm{d}y.$$

If $f(x, y) = 1$ over the aperture then

$$v = \int_{-\infty}^{+\infty} \exp[i(xk_x + yk_y)]\mathrm{d}x\mathrm{d}y = \int_{-\infty}^{+\infty} \psi\,\mathrm{d}x\mathrm{d}y.$$

It can be easily shown that

$$\frac{\partial^2\psi}{\partial x^2} + \frac{\partial^2\psi}{\partial y^2} + (k_x^2 + k_y^2)\psi = 0.$$

Hence

$$v = -\frac{1}{k^2}\int_{-\infty}^{+\infty} \nabla^2\psi\,\mathrm{d}x\mathrm{d}y$$

where

$$k = (k_x^2 + k_y^2)^{1/2}$$

From Green's theorem in two dimensions, we get

$$v = -\frac{1}{k^2}\int_{-\infty}^{+\infty} \frac{\partial\psi}{\partial n}\mathrm{d}s$$

$$= -\frac{1}{k^2}\int_{-\infty}^{+\infty} k_n \exp(ik\cdot r)\mathrm{d}s$$

Here k_n is the component of k that lies in the surface and is normal to the line element $\mathrm{d}s$ of the boundary of the aperture.

Laue (1936) used this result to easily account for the observed Fraunhofer diffraction patterns of triangluar and hexagonal apertures. Ramachandran (1944) using Raman's method arrived at the same answer. He using the stationary phase approximation further simplified the contour integral to contributions from a finite number of points on the boundary. Using a very similar procedure, Mitra (1920) worked out the Fraunhofer pattern for a semicircular aperture.

2.3 *Phases of pole radiations*

We may get an impression that the diffraction pattern can be worked out completely once *poles* where the phases are stationary have been located. But this is far from true. It was pointed out by Ramachandran (1945) that in principle contributions from the points in the immediate neighbourhood of these poles should also be considered. He employed the Cornu spiral method to work out the net contribution from all such neighbouring points. He got a very important result as regards the phases of these pole radiations. Radiation from a pole will have a phase advance of $\pi/4$ or

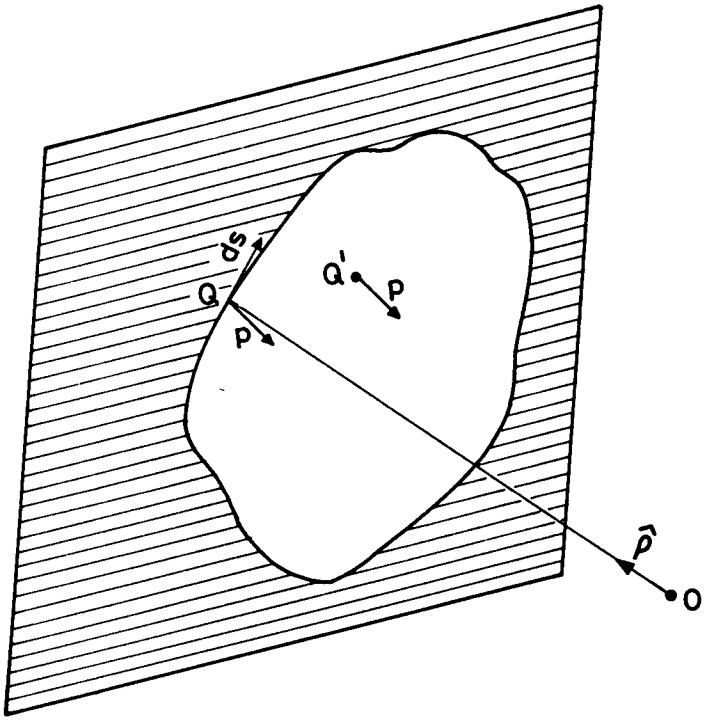

Figure 5. Diffraction at an aperture of an arbitrary shape. The vector **p** is in the direction of incident light. At point Q' where $\hat{\rho} = -\mathbf{p}$, the vector potential **W** becomes singular.

phase lag of $\pi/4$ (all these extra phases are with reference to the phase of pole radiation calculated previously) depending upon whether the pole is one of maximum or minimum path with respect to the point of observation.

Miyamoto and Wolf (1962) interestingly arrived at the same conclusion using Kirchhoff's integral as explained below. The geometry is depicted in figure 5. The Kirchhoff's integrand for any incident vibration u is given by

$$I = \frac{1}{4\pi}\left[u\nabla\left(\frac{\exp(ik\rho)}{\rho}\right) - \frac{\exp(ik\rho)}{\rho}\nabla u\right].$$

Since $\nabla \cdot I$ vanishes we can write I as a curl of a vector potential **W**. For any incident field $u(r') = A(r')\exp[ik\psi(r')]$, we get

$$\mathbf{W}(r', r) = u(r')\frac{\exp(ik\rho)}{4\pi\rho}\frac{\hat{\boldsymbol{\rho}} \times \mathbf{p}}{1 + \hat{\boldsymbol{\rho}} \cdot \mathbf{p}}$$

where $\hat{\rho}$ is a unit vector along ρ and $\mathbf{p} = \nabla'(\psi)$ and r' and r are the position vectors of a point on the aperture and the point of observation. Then

$$v_d = u^B(r) + \Sigma_j F_j(r)$$

with

$$u^B(r) = \int \mathbf{W} \cdot \mathbf{ds}$$

and

$$F_j(r) = l\,t \int_{C_j} \mathbf{W}\cdot\mathbf{ds}$$

C_j's being small circles surrounding singularities of **W** on the aperture.

It can be shown that $u^B(r)$ gives the boundary radiation and F_j's contribute only when the point of observation is in the *illuminated* region where they give the direct beam.

When $u^B(r)$ is evaluated using the stationary phase method we get in the asymptotic approximation

$$u^B(r) = \frac{\exp(\pm i\pi/4)}{\sqrt{k}} \sum_j u(r'_j) \frac{\exp(ik\rho_j)}{4\pi\rho_j} \left[\frac{2\pi}{\partial^2(\rho+\psi)/\partial s^2}\right]_j^{1/2} \frac{(\hat{\boldsymbol{\rho}}\times\mathbf{p})\cdot\mathbf{ds}}{1+\hat{\boldsymbol{\rho}}\cdot\mathbf{p}}.$$

We take the positive or the negative sign according as $[\partial^2(\rho+\psi)]/\delta s^2$ is positive or negative. This gives essentially the Ramachandran phase $\pm\pi/4$ for the poles.

2.4 *Corner radiation*

In the case of obstacles and apertures having sharp corners it is not enough to work out the pole contribution. The procedure used for locating poles, i.e., the method of stationary phases fails when there are sudden changes in curvature. But contributions from such points cannot be ignored either. Kathavate (1945) concluded on experimental grounds that such sharp points act as point sources emitting spherical waves. It should be remarked that many years later Miyamoto and Wolf (1962) arrived at the same conclusion by using the Kirchhoff's integral. In the neighbourhood of such points we find the corner radiation to be given by*

$$u_c = \frac{i\lambda \sin\psi}{4\pi} \frac{\cos(n,r)}{r} \exp(-ikr) \frac{z^2}{d_1 d_2}$$

ψ = angle between the two local tangents to the boundary at the corner

z = the perpendicular distance from the point of observations to the source

d_1, d_2 = components of the vector joining the foot of the perpendicular to the corner.

2.5 *Surface diffraction*

So far we have considered diffraction at infinitely thin apertures and obstacles. But in reality the lateral thickness cannot be ignored. In examples involving three-dimensional objects like cylinders and spheres this lateral dimension will very significantly alter the diffraction phenomena. Raman and Krishnan (1926) were probably the first to draw attention to the fact that spheres and discs behave differently in diffraction. Similarly diffraction at cylinders is very different from diffraction at strips of equal width.

*We are thankful to Prof. R. Nityananda for discussion on corner radiation.

It is well known that in the shadow of a circular disk we get a bright central spot—the Poisson spot. A very similar bright spot is also seen behind a sphere. But Raman and Krishnan found that the central bright spot obtained in the case of the sphere is always less intense than Poisson spot of a circular disk of equal diameter. Only at very large distances the two intensities are nearly equal. These authors accounted for this observed feature by postulating that light rays *creep* around the spherical surface, always leaving the surface along the local tangent. Thus at any point on the axis behind the sphere we get light from a circle on the sphere which is the rim of the tangent cone to the sphere from the point of observation. The ratio of the intensity of the central spot of a disk to that of the sphere of equal diameter decreases exponentially to unity as we recede from the sphere. By employing the Riemann–Weber (1927) analysis of electromagnetic waves propagating around the earth, these authors quantitatively explained this exponential decrease in intensity. According to this model the amplitude damping of the electromagnetic wave after it has a creep angle of θ is given by $\exp[-(0{\cdot}70)\theta(2\pi R/\lambda)^{1/3}]$.

Many years later Keller (1956) independently attacked the same problem and got a very similar answer. The amplitude damping term is in the form of a series given by

$$\sum_{n=1} (D_n)^2 \exp(-\alpha_n R\theta).$$

With

$$\alpha_n = \frac{q_n}{R}\left(\frac{\pi R}{\lambda}\right)^{1/3} \exp(i\pi/6)$$

$$(D_n)^2 = (\lambda/4\pi^2)^{1/2}\left(\frac{\pi R}{\lambda}\right)^{1/3} \exp[-i(\pi/12)] \frac{1}{[A_i'(-q_n)]^2}$$

for the electric vector parallel to the surface and for the electric vector perpendicular to the surface

$$\alpha_n = \frac{q_n'}{R}\left(\frac{\pi R}{\lambda}\right)^{1/3} \exp(i\pi/6)$$

$$(D_n)^2 = \sqrt{\frac{\lambda}{4\pi^2}}\left(\frac{\pi R}{\lambda}\right)^{1/3} \frac{\exp(-i\pi/12)}{q_n'[A_i(-q_n')]^2}.$$

Here q_n is a zero of the Airy function $Ai(x)$ and q_n' is zeros of the derivative of the Airy function $A'(x)$. We easily recognize the Raman and Krishnan solution obtainable as the leading term of the series.

3. Generalized Fermat principle

Keller (1962) suggested an interesting way of unifying all the above different cases. In geometrical optics, the light ray obeys Fermat's principle choosing in refraction or reflection a path for which $\int \mu ds$ is an extremum. In a similar way Keller accounted for the above results by postulating that the light ray is always so diffracted that the total path from the source to the diffracting boundary and from there to the point of observation is an extremum. The path of the diffracted ray can thus be easily

worked out. This generalization of Fermat principle naturally leads to cylindrical or conical edge waves at straight edges. At sharp corners it predicts spherical waves. Even light creeping at surfaces is a consequence of this principle. Also this process predicts that on a cylindrical object light will creep on an helix for oblique incidence.

But a complete solution of the problem of diffraction not only needs the paths taken by the diffracted rays but also their amplitudes. Keller appeals to the results of the previous section, in particular the Sommerfeld edge diffraction, to get in each case these strengths of diffracted rays. For example the diffracted rays for a parallel beam incident at an anlge α, on a straight edge are given by

$$U = U_i D_0 \frac{\exp(ikr)}{\sqrt{r}}$$

with

$$D_0 = -\frac{\exp(-i\pi/4)}{2(2\pi k)^{1/2}\sin\alpha}\left\{\frac{1}{\cos[(\phi-\phi_0)/2]} \mp \frac{1}{\cos[(\phi+\phi_0)/2]}\right\}$$

and U_i is the incident wave.

The diffracted rays will be travelling on the surface of a cone symmetric about the edge (figure 3). Keller also worked out the diffraction when the edge is not straight but has finite curvature. He argued that a local cylindrical wave will be emitted by the boundary. Thus the emerging wave front will also be locally curved parallel to the edge. From light flux conservation Keller showed that the diffracted rays in such a case are given by

$$U = D_0 U_i \frac{\exp(ikr)}{\left[r\left(1+\frac{r}{\rho_1}\right)\right]^{1/2}}$$

where ρ_1 denotes the distance from the edge to the caustic of diffracted rays measured negatively in the direction of propagation. Hence as we cross the caustic U gets an extra phase of $\pi/2$, and the expression itself is not valid at and near the caustic.

We can also easily understand why only a few selected points of the boundary should contribute to the net diffraction field at any given point. The path from the source to the point of observation via the boundary will be an extremum only at these points on the boundary. Hence the generalized Fermat's principle naturally leads to the notion of pole radiations. It is for these reasons the boundary wave theory of diffraction has come to be known as the Geometrical Theory of Diffraction (GTD).

Thus the problem of diffraction reduces to finding the extremum paths for the diffracted rays and then incorporating the amplitude for each such diffracted rays. At any point of observation we add with appropriate phases all these diffracted rays to get the net vibration.

4. Applications of GTD

It was said earlier that the Kirchhoff-Helmholtz diffraction is not amenable to calculations even in simple geometries. It is in this context that the GTD acquires a new significance. Though in the beginning GTD was considered as a different model

of diffraction, later developments and refinements evolved out of the realization that GTD could be an effective and powerful method in calculating diffraction patterns. However here we will be using GTD not to highlight these features but to account for peculiar features associated with certain diffraction patterns and to suggest solutions in situations where the Kirchoff theory is virtually powerless.

4.1 *Transparent and semitransparent laminae*

We have already mentioned the work of Raman and Krishnan (1927) on metallic screens wherein they generalized the Sommerfeld solution. Later Raman and Rao (1927) extended the same theory to account for diffraction at thin transparent laminae. This problem naturally arose out of earlier experimental work of Raman and Ghosh (1918) on the diffraction at boundaries of mica and of Raman and Banerji (1921) on the colours of mixed plates. They considered the geometry where light fell normally on the diffracting edge. There will be three regions in the light field: 1. Region of light transmitted by lamina alone; 2. Region of incident light; 3. Region of superposition of incident and reflected light.

They constructed a solution which not only satisfied the wave equation but also smoothly and asymptotically reached the solutions at the previously mentioned regions. Their solutions for the electric vector parallel and perpendicular to the edge respectively are given by

$$E_z = \frac{i^{3/2}\exp(-ikr)}{4\pi(r/\lambda)^{1/2}}\left[\frac{1-(C+iD)}{\cos(\phi-\phi_0)/2} - \frac{A+iB}{\cos(\phi+\phi_0)/2}\right]$$

$$H_z = \frac{i^{3/2}\exp(-ikr)}{4\pi(r/\lambda)^{1/2}}\left[\frac{1-(C'+iD')}{\cos(\phi-\phi_0)/2} + \frac{A'+iB'}{\cos(\phi+\phi_0)/2}\right].$$

Here $(A+iB)$ and $(C+iD)$ are the reflection and transmission coefficients of the lamina. In calculating these quantities multiple reflections are taken into account. They are given by (for normal incidence)

$$A+iB = A'+iB' = \frac{i(\mu^2-1)\sin kt}{i(\mu^2+1)\sin kt + 2\mu\cos kt}$$

$$C+iD = C'+iD' = \frac{2\mu(\cos k_0 t + i\sin k_0 t)}{i(\mu^2+1)\sin kt + 2\mu\cos kt}$$

μ = refractive index, t = lamina thickness, $k = 2\pi\mu/\lambda$, $k_0 = 2\pi/\lambda$.

Interestingly the very same solution was arrived at very recently by Burnside and Bergener (1983), who were unaware of the earlier work.

Ananthanarayanan extended the above theory to metallic films by making μ complex (Ananthanarayanan 1940). He used this to account for his experimental observations on the diffraction at thin metallic films. In this case he not only found a fringe system in the shadow region, but they were also of better clarity compared to fringes in the *light* region. He explained this observation by arguing that the cylindrical edge wave emanating from the straight boundary interferences with the wave weakly transmitted by the metallic film. The higher contrast is due to the fact that these two waves are nearly of comparable intensity. On the *illuminated* side the main beam is far more intense compared to the intensity of the cylindrical edge wave resulting in fringes of low visibility.

4.2 *Apertures and obstacles with straight edges*

We have already solved the diffraction problem at a straight edge. We now extrapolate the results obtained there to apertures and obstacles bounded by straight edges. When a plane wavefront, i.e., parallel beam of light falls on such an object, each of the straight edges will emit cylindrical waves, i.e., rays radiating out in all directions but normal to the edge. Any point within the shadow gets these cylindrical waves. They will have to be added with strengths (i.e., the diffraction coefficient) given by D_0 and with appropriate phases to get the net vibration. Since the diffracted rays are normal to the straight edges, any point of observation gets edge radiation only from a few points, i.e., poles on the boundary of the object. These poles are located at the feet of the perpendiculars drawn to the straight edges, from the point of observation. As the point of observation changes the location of the poles also will change. For points in the illuminated region we have to have in addition the main wave as well.

As Kathavate (1945) pointed out, this geometrical exercise can be further simplified to work out the diffraction pattern in these problems. On the plane of observation we locate the geometrical shadow boundary of the object. From the point of observation, which is on this plane, we drop perpendiculars to the shadow boundaries. The feet of these perpendiculars on this projected plane correspond to the projection of poles on the shadow boundary. It is a matter of elementary algebra to work out the path differences between the various pole radiations reaching any point of observation. We get some interesting results in the diffraction of a plane bonded by two straight edges, but at an angle. When this angle is acute every point in the shadow regions gets two pole radiations one from each edge. Hence we have hyperbolic fringes in the area of the geometrical shadow. On the other hand, if the angle between the edges is obtuse, then only in a smaller sector of an acute angle (which is complementary to the obtuse angle) within the shadow we get at any point, radiations from both the edges. Outside this region, but within the shadow boundaries, we have only one side sending out radiations to the point of observation. Hence in such obtuse angle geometries we get hyperbolic fringes inside the inner acute angle sector surrounded by weak field. In the case of a parallellogram, however, we find a small inner parallellogram (defined by the area between the perpendiculars drawn to the four boundaries) within which all the four sides, i.e., four poles, contribute. Then there is a region with only two pole contributions. In addition, near the tips of obtuse angular edges we have only one pole radiation. Hence the central parallellogram shines out with a network of fringes. Kathavate (1945) beautifully demonstrated these features of diffraction in such geometries.

All such objects which are bounded by straight edges, also have sharp corners. We have already mentioned that such corners act independently as sources of spherical waves diverging in all directions. Hence we have to add the cylindrical waves from poles and spherical waves from corners. But in certain regions of the diffraction pattern, we can clearly see the effect of corner waves. In the case of a square sector, near an edge, the pole radiations and corner raditations interfere to give a fringe pattern perpendicular to the edge. In fact Kathavate, who experimentally found these features, suggested corner spherical waves to account for his observations. In figure 6 we give Kathavate's construction for a rectangular sector. This accounts for the appearance of fringes perpendicular to an edge. Also in certain illuminated regions we find the corner wave to yield circular fringes due to its interference with the main wave. In these regions we have no pole radiations.

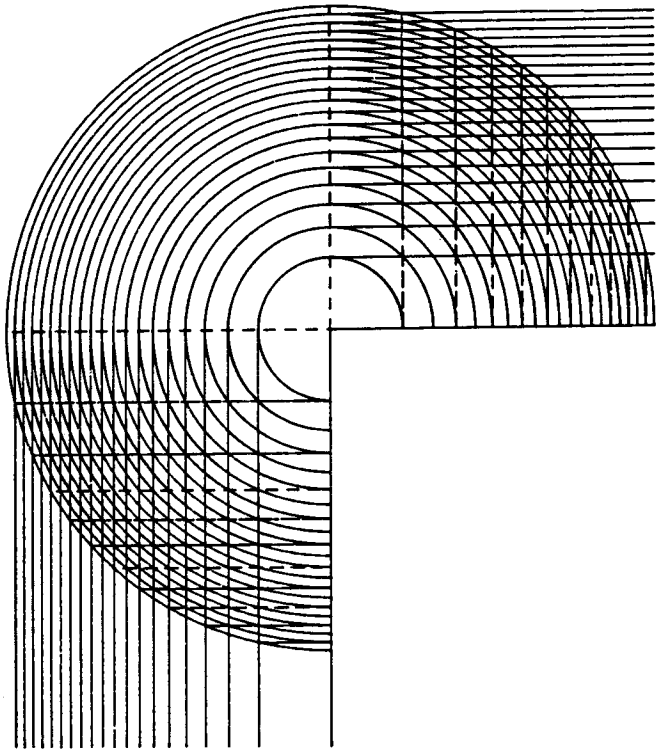

Figure 6. Kathavate's geometrical construction for a rectangular sector in the shadow region. The lines parallel to the edges are the lines of equal phase difference for the cylindrical waves from the edges. The circles are the lines of equal phase difference for the spherical wave from the corner. The broken lines perpendicular to the edge indicate the position of the dark fringes due to the interference between the corner waves and the edge waves.

We show in figure 7a the diffraction pattern computed using GTD for an equilateral triangular aperture, with pole radiations only. In figure 7b we show the same but with effects due to corner waves.

4.3 *Apertures and obstacles with curved edges*

In these geometries an incident plane wavefront falling normally on the object results in a local cylindrical boundary wave which is also laterally curved due to the curvature of the edge. Here also the edge diffracted waves will diverge in directions that are normal to the local tangent. Hence there will be concentration of light along the evolute to the boundary to which these boundary diffracted rays are tangential. In the diffraction pattern this evolute will stand out conspicuously. Raman (1919, 1941) who was probably the first to study them, called them *Diffraction Caustics* in view of the similarity they bear with normal caustic formation in geometrical optics. Mitra (1919) made a detailed study of these caustics in different cases like apertures and disks with corrugated boundaries. In each case he accounted for their existence by invoking boundary radiations, and argued that the diffraction caustics are to be found along the evolute to the boundary. Coulson and Becknell (1922) arrived at the same

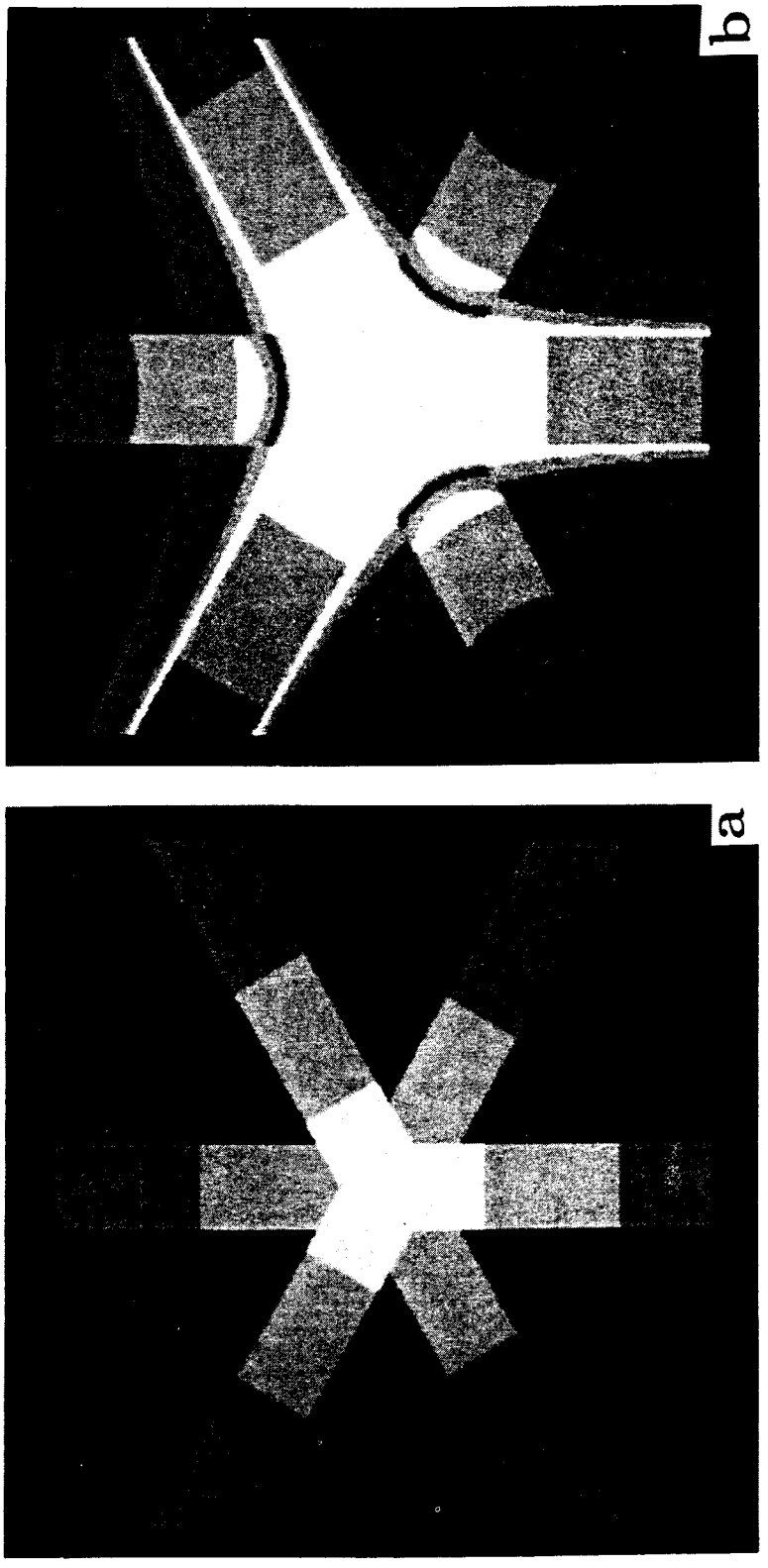

Figure 7. The simulated diffraction pattern for an equilateral triangular aperture of side 0·05 cm at a distance of 100 cm. (**a**) with pole radiations only, (**b**) with pole and corner radiations. Sharp steps in intensity in this and the later pictures are an artifact of intensity steps selected during the calculations. In reality, however, there is always a smooth variation in intensity.

conclusions by studying opaque disks of various shapes. Many years later Nienhuis (1948) undertook a similar study for apertures of different shapes and found diffraction caustics to result from boundary radiations. It may be remarked that for circular boundaries the evolute degenerates to a bright point at the centre, first predicted by Poisson.

In addition to these bright lines there are other features associated with the diffraction pattern which can again be easily accounted for by GTD. For example, in the case of a circular disk at points away from the centre but within the shadow, we find two boundary radiations emanating from the diametrically opposite poles on either side. They have to be added with their proper phase differences. While doing this addition we must also include the Ramachandran phase of $\pm \pi/4$ at each pole. Thus we can expect a system of concentric bright circular fringes. On any one such circular fringe the two pole radiations are in phase. In the case of an elliptic disk we find 4 poles to contribute to any point within the evolute while for points beyond the evolute but within a shadow boundary we have two pole radiations. Using Keller's diffraction coefficient D we can get the diffraction pattern for any object with a curved boundary. In figures 8 and 9 we have presented our calculated diffraction pattern using GTD for an elliptic disk and elliptic aperture. We find a network of fringes within the evolute. Our calculations are in qualitative agreement with the observations of Kathavate (1945).

All the above arguments are valid if and only if the curvature changes smoothly over the boundary of the obstacle. If however there are sudden changes in curvature then such points act like additional sources of light emitting spherical waves. The diffraction coefficient is again given by the formula worked out earlier for corners. Sharp points where curved edges meet have the value of the diffraction coefficient same as that obtained for a corner with straight edges.

4.4 *Poisson spot*

We have already mentioned the existence of a bright central spot in the case of circular disks. This arises due to the constructive interference of the boundary waves at the centre. With the diffraction coefficient D given previously for curved edges we get an infinite intensity at the centre. Keller (1962) has overcome this difficulty by correcting

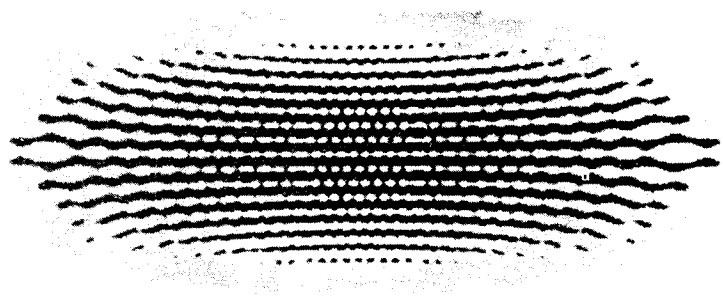

Figure 8. The simulated diffraction pattern for an elliptic disk (major and minor diameters 1 cm and 0·4 cm respectively) at a distance of 100 cm.

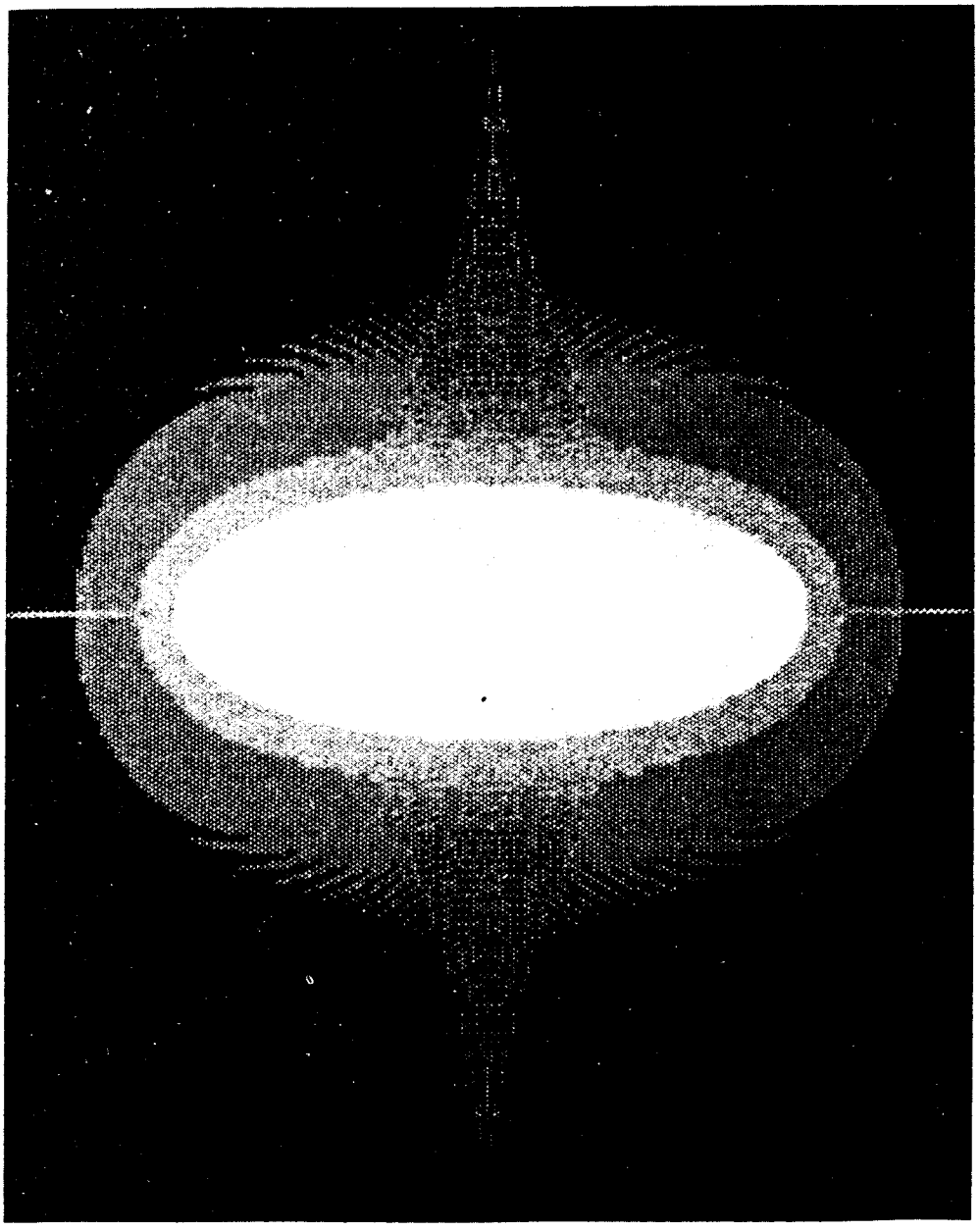

Figure 9. The simulated diffraction pattern for an elliptic aperture of the same dimensions used in figure 8.

D which gives good agreement with the exact theory in the far field, i.e., Fraunhofer limit.

In other geometries also we get a central spot whose features can be worked out using GTD. Firstly we get an infinite number of rays reaching such a spot only for circular boundaries. For any other shape of the boundary we find a finite number of points on the boundary contributing to the centre. Hence the central spot in every

other geometry will be weaker than the classical Poisson spot. This accounts for the experimental observation of English and George (1988) who found the central spot in the case of a square disk to be far weaker than what one finds for a circular disk. In this case four poles situated respectively at the centres of the four edges send out cylindrical waves to the centre. In addition, we also have four corner radiations. Thus only eight points on the boundary contribute to the central spot. It is also important to realize that the four pole radiations are in phase at the centre and the four corner radiations are also in phase at the centre. But the pole and corner radiations need not be in phase. The exact phase difference depends upon where we are on the central axis. In principle they will successively be in and out of phase as we recede from the plane of the square disk, thus resulting in fluctuations in the central spot intensity. In practice, however, this may not be conspicuous due to the fact that the corner radiations fall of as $1/r^2$ in intensity while the pole radiations fall off as $1/r$ in intensity.

However, an interesting possibility exists for rectangular and elliptic disks. In both the cases we have four pole radiations contributing to the centre. In the case of the rectangle we also have the corner radiations. But their contributions can be ignored due to their weak strengths. Thus in both the geometries we have four pole radiations. Two of the opposite pole radiations are in phase at the centre. Similarly the other

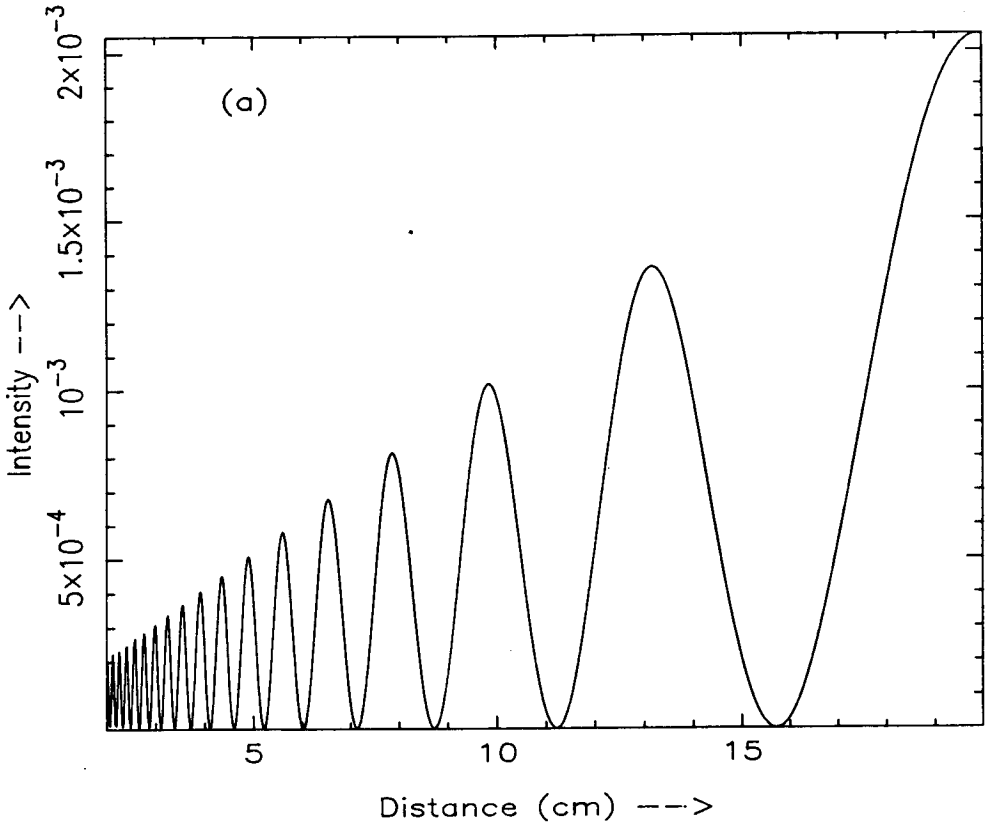

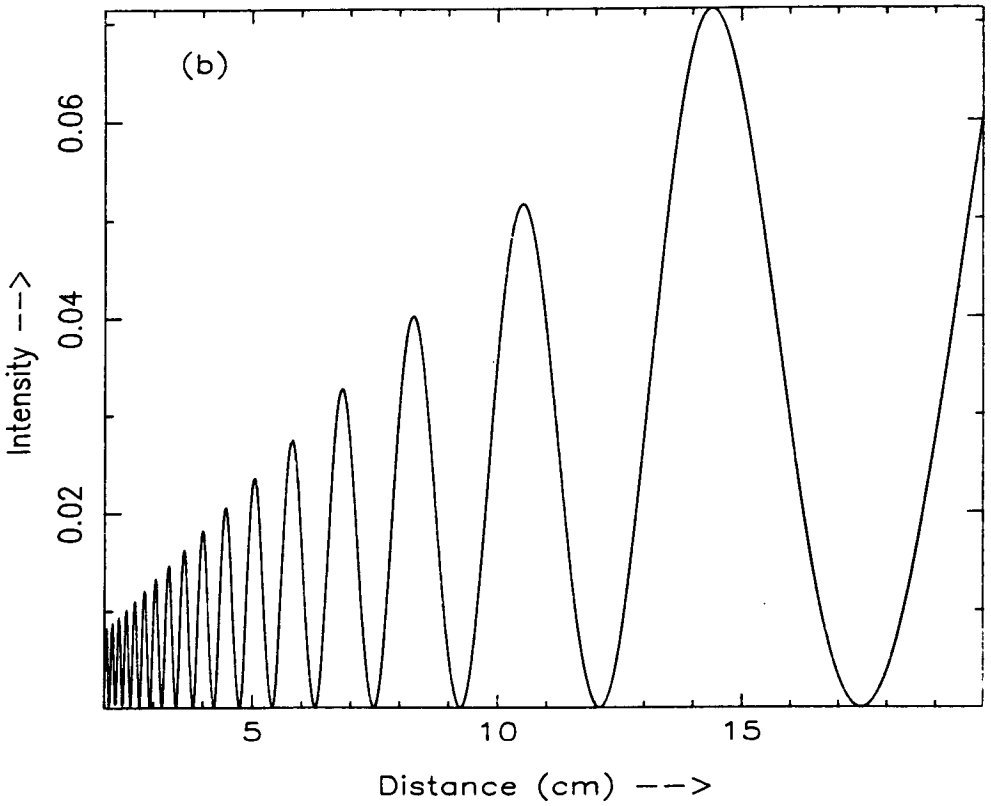

Figure 10. Dependence of Poisson spot intensity with distance from the diffracting screen for (**a**) rectangular obstacle with length 1 cm and breadth 0·99 cm. (**b**) elliptic disk of major dia 1·0 cm and minor dia 0·99 cm.

set of opposite pole radiations are also in phase. But these two pair of pole radiations will be in and out of phase as we recede from the plane of the object resulting in central spot intensity fluctuation. The same phenomenon will be observable at any given point as the ratio of sides (or axes) changes continuously. We now consider a rectangular disk and an elliptic disk of equal dimensions [i.e., length (breadth) of the rectangle is equal to the major (minor) diameter of the ellipse]. Similar poles in the two cases are situated at the same distances from the central axis. Hence we may conclude that the central spot intensity should be identical in the two cases at any given point on the axis. But a careful study of diffraction coefficients will show that this is not the case. For the rectangle we use the diffraction coefficient D_0 while for the elliptic disk we have to use D which includes the local radius of curvature. Hence the Poisson spot intensities are quite different in the two cases. Also for the elliptic disk one pair of pole radiations will have $\pi/2$ extra phase compared to the other pair of pole radiations since for this pair the central spot will be beyond the radius of curvature at the pole. Thus in many respects the Poisson spots are different in the two cases. In figure 10 we have given calculations pertaining to this comparison between elliptic and rectangular disks.

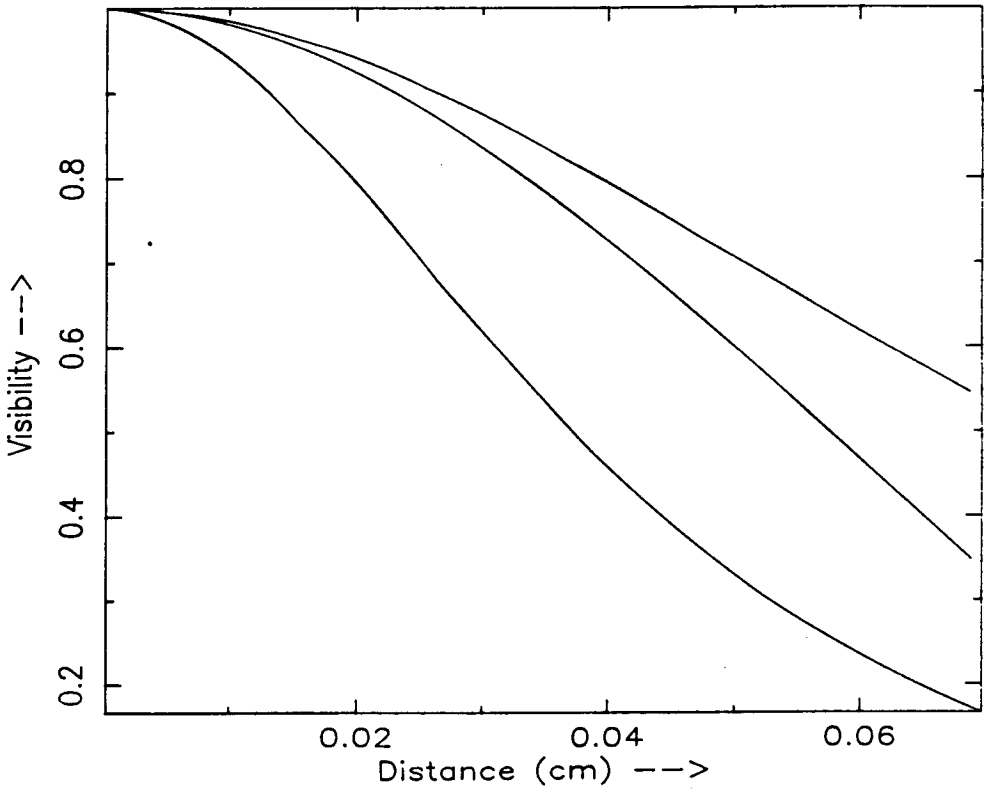

Figure 12. Visibility of the fringe system for a strip and a cylinder. Upper and lower curves are the visibility of the fringe system of a cylinder at a distance of 4 cm and 2 cm respectively. The middle curve shows the fringe visibility of the strip at these two distances. In this case the visibility is independent of the distance from the strip.

Hence the interference pattern obtained in this case would be quite different from that of a strip.

We show in figure 11 results of our calculation of the fringe pattern for the incident electric vector parallel to the edges. We find many interesting differences between the two cases. Firstly fringe spacing and fringe intensities are very different in the two cases. Secondly the visibility of the fringe system is not a constant over the pattern. Also the visibility of the pattern in the case of a cylinder as compared to that of the strip behaves very unexpectedly with distance. This is shown in figure 12. We see the visibility curves to cross over indicating a reversal in the clarity of fringes of a cylinder compared to that in a strip. It should be quite clear from these results that the usual text book argument that the fringe system in the case of cylinder is due to two line sources placed at its outermost edges is a oversimplified picture. Only at large distances do the two fringe patterns agree.

5. Diffraction symmetry

The geometrical symmetry of an aperture or an obstacle influences strongly the symmetry of the diffraction pattern. In addition, the conditions under which one

studies the diffraction pattern also influences the diffraction symmetry. For example symmetry in the Fraunhofer limit is higher than that one gets in Fresnel limit and is obtained by adding a centre of symmetry. The well known example is that of an equilateral triangular aperture. In the Fresnel limit the three fold symmetry of the aperture gets imposed on the diffraction pattern. Thus the Fresnel pattern is non-centrosymmetric. However, in the Fraunhofer limit the same equilateral triangle results in a diffraction pattern of six-fold symmetry which is centrosymmetric. In fact as a general rule, following from the Fourier transform technique, we can say that the Fraunhofer diffraction is always centrosymmetric. In many examples Raman and his students studied this transition from Fresnel to Fraunhofer pattern as the aperture dimension is decreased. This smooth transition from Fresnel to Fraunhofer pattern can also be qualitatively demonstrated using GTD. In figure 13 we have given our calculated diffraction pattern for an equilateral aperture. The transition from 3-fold to 6-fold is clearly evident. However, it should be emphasized that GTD is strictly not valid in the Fraunhofer limit.

Interestingly the diffraction symmetry is also strongly influenced by the polarization of the incident radiation. This special feature of diffraction patterns is easily obtainable from GTD while a rigorous theoretical calculation could be mind boggling. We shall take a square disk as an example to illustrate this point. When the incident wave is linearly polarized parallel to one pair of opposite edges it will be orthogonal to the other pair of edges. From our expression for D_0 we can immediately conclude that the strength D_0 is different for the two pairs of opposite edges. Hence the pattern is not strictly 4-fold symmetric but is 2-fold symmetric. This polarization asymmetry is due to the second term in D_0 whose sign depends on the polarization of incident vibration relative to the edge. In reality, this term contributes significantly only at very small distances from the diffracting screen. Hence the 2-fold symmetry is realizable only at such distances. It must be remarked that the diffraction symmetry is also sensitive to the azimuth of the incident linear vibration. When it is along the diagonal all the four sides will become equivalent resulting in a 4-fold symmetric diffraction pattern. However, for incident unpolarized light the diffraction pattern will have polarization features which will have a 4-fold symmetry for a square lamina. These features are again calculable from GTD.

6. Multiple edge diffraction

The GTD as presented so far is incomplete. The incident wave results in edge waves and corner waves. These waves again travel towards the other edges and corners to result in a second diffraction. This process could go on and on. Hence from each edge or a corner we have a multiplicity of waves. Keller (1957) has calculated these higher order diffraction coefficients. Calculations based on these higher orders indicate that in most cases of interest these higher order diffraction coefficients are unimportant.

7. Diffraction at thick screens

So far we have discussed diffraction at obstacles and apertures of infinitesimally small thickness. In such cases, in principle, we can calculate the diffraction pattern using

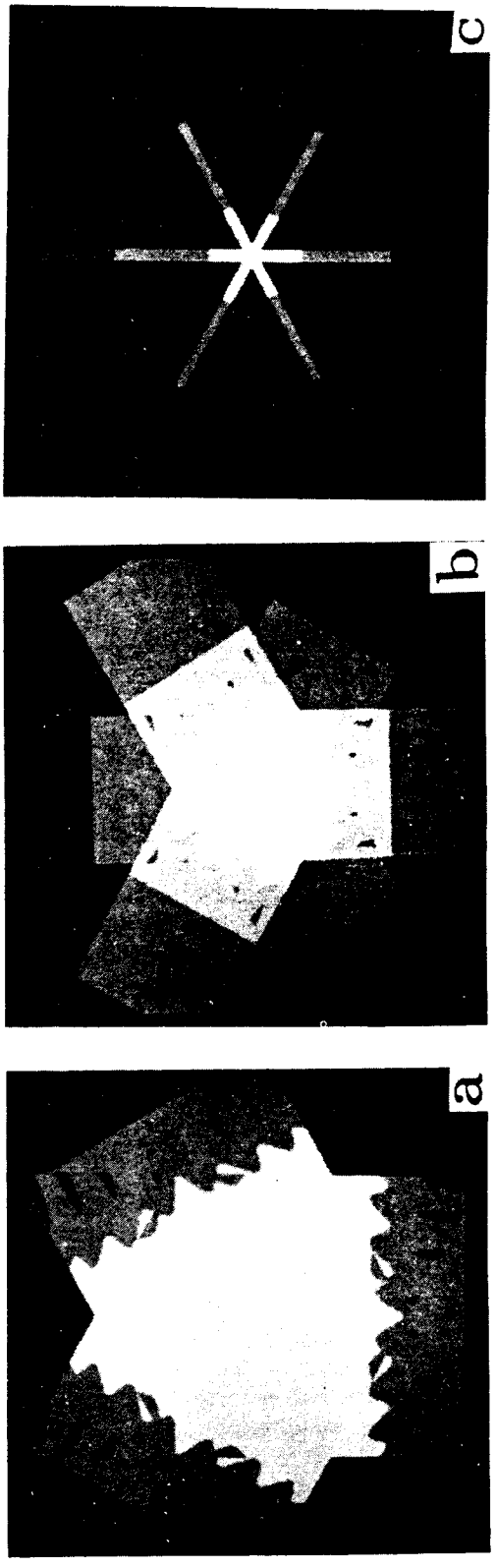

Figure 13. Transition from Fresnel to Fraunhofer pattern for an equilateral triangular aperture as the side decreases. (**a**) 0·25 cm, (**b**) 0·2 cm, (**c**) 0·01 cm at a distance of 100 cm from the aperture.

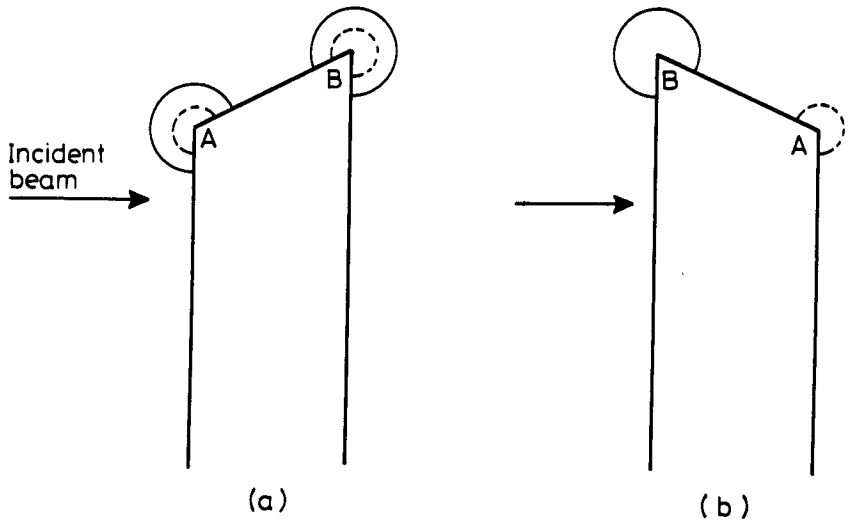

Figure 14. Geometry depicting diffraction at a thick screen with sharp edges.

the Kirchhoff theory. But it is not within the scope of Kirchhoff's theory to yield answers when the screens are of finite thickness. Interestingly, GTD can be effectively used to work out the implications of this lateral thickness of the screen. We shall illustrate this with a few examples.

7.1 *A knife edge*

In this geometry the diffracting edge has a lateral dimension as shown in figure 14a. It has two sharp straight edges seen as A and B in cross section. When a plane wavefront falls normally on the kinfe edge with A turned away from the light rays as in figure 14b, then the edge B acts as a source of cylindrical waves. This cylindrical wave will also reach the other edge A which after receiving this wave will act as a secondary source of cylindrical waves. These secondary waves will be of weaker strength. Hence there are three regions in the diffraction pattern. The region beyond the plane AB has only the wave from A while the region between AB and the normal at B to the front surface has waves from A and B. This results in an interference pattern very much like that in a strip. In the region of geometrically transmitted wave, we have in addition to the cylindrical wave from B, a secondary cylindrical wave from A. Thus the diffraction pattern is truly quite complex yet amenable to analysis by GTD. It must be remarked that if the edge A were to face light as in figure 14a the waves from A will not reach the classical geometric shadow. Secondly B will be a source of two cylindrical waves one due to the direct beam and another cylindrical wave excited by the cylindrical wave from A. Similarly A is also a source of a secondary cylindrical wave. Hence region II of the previous geometry is absent here. Also the shadow region will be brighter since two cylindrical waves both starting from B reaches it. In the region of geometrically transmitted light we have two further regions. One as in the previous geometry with two cylindrical waves in addition to the main beam. Second one has in addition to these three contributions another from the wave reflected by the face AB.

The excitation of the secondary cylindrical wave is a very sensitive function of the polarization of incident light. We can clearly see from the Sommerfeld diffraction coefficient D_0 that the amplitude of the wave vanishes along AB for the electric vector parallel to the edge. Hence for this polarization we do not get the secondary cylindrical wave.

7.2 *Round edges*

In figure 15 we show a straight edge with a round lateral extension which smoothly goes over to another plane face parallel to the front face of the thick screen. When a plane wave point falls on the face with the flat face towards light, then A acts as a source of cylindrical wave. This wave creeps along the smooth surface and sends light at all angles of diffraction. Hence diffraction pattern will be very similar to that of a thin straight edge excepting for the fact that the shadow region gets light through a creeping of the cylindrical wave. Hence it will be less luminous.

If the object is turned around so that the smooth surface is turned towards light then we have only cylindrical waves diverging from A. It will be exactly like that of a stright edge in the shadow region. But in the region of light we have the direct light, the cylindrical wave from A, reflection by the smooth surface. The pattern will therefore be very complicated but can be easily computed using GTD. For oblique incidence the cylindrical wave at A arises due to creeping of light.

We can use similar arguments in other geometries. The procedure is analogous to the multiple diffraction technique of Keller (1957) which we discussed previously.

8. White or polychromatic light diffraction

To get diffraction patterns in white light all that we need to do is to add the intensitites of the diffraction patterns due to the individual components of the incident light. In view of its simplicity one can do this far more quickly with GTD than with Kirchhoff's theory. Also the effects of polarization of incident light can be easily incorporated using GTD.

In figure 16 we show the calculated diffraction pattern of a square disk, with a polychromatic source. It has been compared with the pattern obtained for monochromatic light. In many respects we find a good agreement with the experimental observations of Kathavate (1945) on white light diffraction.

9. Effect of finite conductivity

Raman and Krishnan (1927) introduced in a simple way finite conductivity of the diffracting screen. The second term of the Sommerfeld solution gets multiplied by a complex reflection coefficient. This simple modification neatly accounts for the experimental observations in the case of straight edges. The implications of this modification on the nature of the diffraction pattern will be briefly discussed in this section.

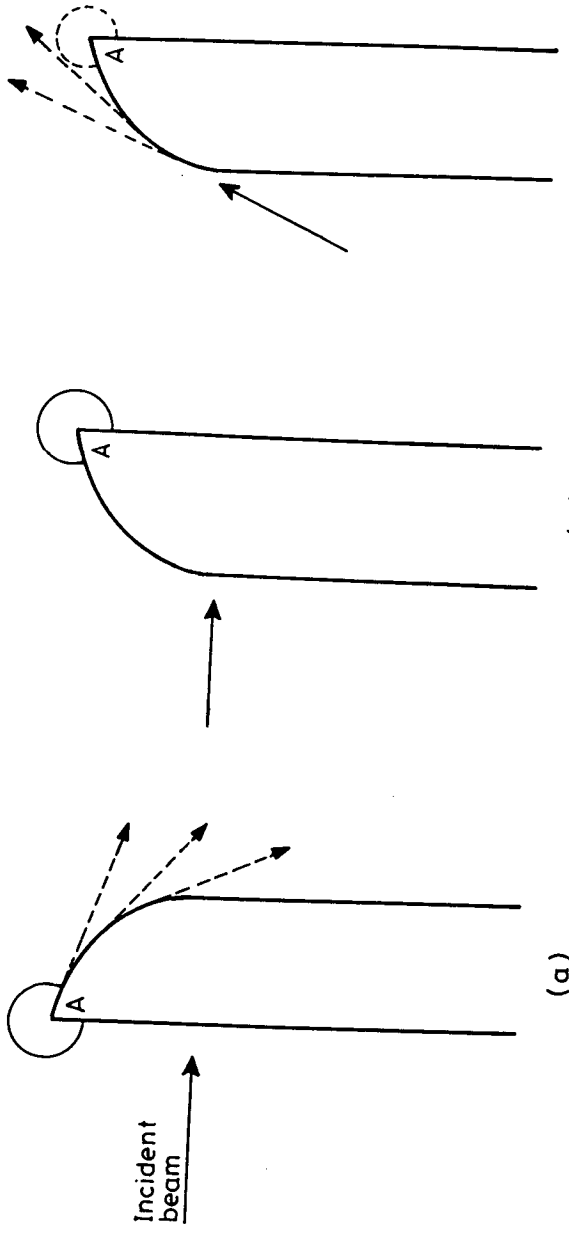

Figure 15. Geometry for the diffraction at a thick screen with a smooth surface and a sharp edge.

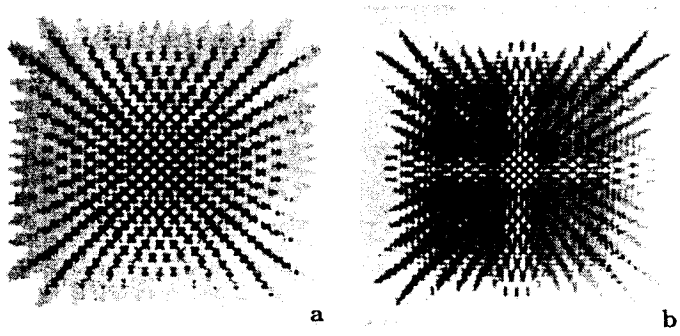

Figure 16. The simulated diffraction pattern in the shadow of a square obstacle of side 0·2 cm at a distance of 50 cm for (a) for a monochromatic light of 650 nm, (b) polychromatic light composed of wavelengths 450 nm, 500 nm, 600 nm and 650 nm.

9.1 *Straight edge*

As Raman and Krishnan (1927) pointed out, the diffracted light is strongly polarized in this situation. And for a general azimuth of incident linear vibration, diffracted light will be in general elliptically polarized. Another interesting aspect of diffraction pertains to fringe formation. In principle according to this theory the phase of the Sommerfeld wave for the electric vector parallel to the edge is not the same as its phase when the electric vector is perpendicular to the edge. As a consequence the fringe positions will be different in the two cases.

9.2 *Poisson spot*

In the case of a square disk we pointed out that the central maximum, i.e., the Poisson Spot can exhibit fluctuations in intensity as we recede from the screen. But it was also emphasized that these fluctuations would generally be too weak to be observable due to the weak contribution from corners. If finite conductivity is taken into account, then with a linear vibration parallel to one pair of edges, we find the two pairs of edges wave to diverge out with different phases. Hence due to this alone one must have intensity fluctuations in the central spot.

9.3 *Thick screens*

In problems involving thick screens we meet situations where the Sommerfeld wave undergoes a second diffraction at another edge or corner. When conductivity is infinite such a processes would be absent for the electric vector parallel to the first edge at which the primary wave was generated. However, in the case of finite conductivity this is not so. Hence the diffraction patterns are in generally different in this case.

10. Conclusions

We have reviewed the basic concepts and results of the geometrical theory of diffraction. This approach to problems involving diffraction is not widely known or

appreciated even though it has many technical advantages over the conventional theories. In addition, it offers simple and elegant explanations for many of the interesting features associated with diffraction patterns. We have applied this technique to a few geometries to bring out the power of this method.

Acknowledgements

We are thankful to Prof. S Ramaseshan for many stimulating discussions we had with him. We also acknowledge Prof. R. Nityananda for helpful suggestions and comments.

References

Ananthanarayanan N 1940 *Proc. Indian Acad. Sci.* **A10** 477
Banerji S K 1919 *Philos. Mag.* **37** 112
Burnside W D and Bergener K W 1983 *IEEE Trans.* **31** 104
Coulson J and Becknell G G 1922 *Phys. Rev.* **20** 594
English R E and George N 1988 *Appl. Opt.* **27** 1581
Kalaschnikow 1912 *J. Russ. Phys. Soc.* **44** 133
Kathavate Y V 1945 *Proc. Indian Acad. Sci.* **A21** 177
Keller J B 1956 *IRE Trans. Antennas and Propagation* **AP24** 312
Keller J B 1957 *J. Appl. Phys.* **28** 426
Keller J B 1962 *J. Opt. Soc. Am.* **52** 116
Kouyoumjian R G and Pathak P H 1974 *Proc. IEEE Trans.* **62** 1448
Laue Von. M 1936 *Berliner Sitzungsberichte* p. 89 (see also Jame R W 1967 *The optical principles of the diffraction of X-rays* (G. Bell and Sons Ltd.)
Maey E 1893 *Ann. Phys.* (Lpz) **49** 93
Maggi G A 1888 *Ann. di. Mat.* **11a** 16
McNamara D A, Pistorius C W I and Malherbe J A G 1990 *Introduction to uniform geometrical theory of diffraction* (Artech House, Norwood) and references therein
Mitra S K 1919 *Philos. Mag.* **38** 289
Mitra S K 1920 *Proc. Indian Assoc. Cultiv. Sci.* **6** 1
Miyamoto K and Wolf E 1962 *J. Opt. Soc. Am.* **52** 615, 626
Nienhuis K 1948 *Thesis, Gröningen*
Ramachandran G N 1944 *Proc. Indian Acad. Sci.* **A19** 123
Ramachandran G N 1945 *Proc. Indian Acad. Sci.* **A21** 165
Raman C V 1919 *Phys. Rev.* **13** 259
Raman C V 1941 *Sayaji Rao Gaekwar foundation lectures on physical optics* (Indian Academy of Sciences) Published in 1959
Raman C V and Banerji B N 1921 *Philos. Mag.* **41** 338
Raman C V and Ghosh P N 1918 *Nature (London)* **102** 205
Raman C V and Krishnan K S 1926 *Proc. Phys. Soc. (London)* **38** 350
Raman C V and Krishnan K S 1927 *Proc. R. Soc. (London)* **A116** 254
Raman C V and Ramakrishna Rao I 1927 *Proc. Phys. Soc. (London)* **39** 453
Riemann-Weber 1927 *Differential Gleichungen Phys.* **2** 594
Rubinowicz A 1917 *Ann. Phys.* **53** 257
Rubinowicz A 1924 *Ann. Phys.* **73** 339
Savornin J 1939 *Ann. Phys.* **11** 129
Sommerfeld A 1896 *Math. Ann.* **47** 317
Sunil Kumar P B and Ranganath G S 1991 *Curr. Sci.* **61** 22
Young T 1802 *Philos. Trans. R. Soc. (London)* **20** 26